Received: 29 March 2017 | Revised: 30 August 2017 | Accepted: 5 September 2017

DOI: 10.1002/cne.24323

RESEARCH ARTICLE

WILEY The Journal of Comparative Neurology

Cre-expressing neurons in visual cortex of Ntsr1-Cre GN220 mice are corticothalamic and are depolarized by acetylcholine

Sofie Charlotte Sundberg | Sarah Helen Lindström | Gonzalo Manuel Sanchez | Björn Granseth

Department of Clinical and Experimental Medicine (IKE), Faculty of Medicine, Linköping University, Linköping, Sweden

Correspondence
Björn Granseth, Department of Clinical and Experimental Medicine (IKE), Faculty of Medicine, Linköping University, 581 85 Linköping, Sweden
Email: bjorn.granseth@liu.se

Abstract

The Ntsr1-Cre GN220 mouse expresses Cre-recombinase in corticothalamic (CT) neurons in neocortical layer 6. It is not known if the other major types of pyramidal neurons in this layer also express this enzyme. By electrophysiological recordings in slices and histological analysis of the uptake of retrogradely transported beads we show that Cre-positive neurons are CT and not corticocortical or corticoclaustral types. Furthermore, we show that Ntsr1-Cre-positive cells are immuno-positive for the nuclear transcription factor Forkhead box protein P2 (FoxP2). We conclude that Cre-expression is limited to a specific type of pyramidal neuron: CT. However, it appears as not all CT neurons are Cre-expressing; there are indications that the penetrance of the gene is about 90%. We demonstrate the utility of assigning a specific identity to individual neurons by determining that the CT neurons are potently modulated by acetylcholine acting on both nicotinic and muscarinic acetylcholine receptors. These results corroborate the suggested function of these neurons in regulating the gain of thalamocortical transfer of sensory information depending on attentional demand and state of arousal.

KEYWORDS

acetylcholine, corticothalamic, claustrum, FoxP2, Ntsr1, visual cortex, RRID: MMRRC_030648-UCD, RRID: AB_10000240, RRID: AB_2313516, RRID: AB_2107107, RRID: SCR_002074

1 | INTRODUCTION

Cre-lox recombination has become a widely-used technique for studying specific cell types and has proved particularly useful for untangling neuronal circuits in the brain. Ntsr1-Cre GN220 is a transgenic mouse line carrying an intron containing a Cre cassette inserted into a bacterial artificial chromosome (BAC) vector for the neurotensin receptor type 1 (Ntsr1) (Gong et al., 2007). In the neocortex, Cre-recombinase expression seems to be limited to about two thirds of the pyramidal neurons in the deepest neocortical layer, layer 6 (Gong et al., 2007; Olsen, Bortone, Adesnik, & Scanziani, 2012). Layer 6 contains three different classes of pyramidal neurons that can be distinguished by their projections: the corticothalamic (CT) neurons that project to the thalamus, the corticocortical (CC) neurons with axons that do not leave the neocortex, and the corticoclaustral (CCl) neurons that project to the claustrum (Reviewed in Thomson, 2010). CT neurons are known to express Cre in Ntsr1-Cre GN220 mice (Crandall, Cruikshank, & Connors, 2015; Gong et al., 2007; Kim, Matney, Blankenship, Hestrin, & Brown, 2014; Olsen et al., 2012), but whether CC and CCl neurons are also Cre-expressing remains to be investigated.

Even though the agonist, neurotensin has no apparent effect on neurons in this neocortical layer (Case, Lyons, & Broberger, 2016), measurements of mRNA for Ntsr1 indicate that Ntsr1-Cre positive neurons express the *NTSR1* gene, albeit at a low level (Tasic et al., 2016). When a gene with low expression is used for driving Cre the risk of partial expression of Cre increases (i.e., Cre will not be expressed in all cells in a population). If, and to what extent, partial expression occurs in the Ntsr1-Cre GN220 mouse has not previously been investigated. If all three classes of layer 6 pyramidal neurons are found among the cells expressing Cre-recombinase, partial expression must be substantial. If only CT neurons are Cre-positive, partial expression should be of minor consequence.

By examining electrophysiological characteristics and the pattern of retrograde transport of fluorescent beads, we establish that Cre-expression is specific for CT neurons and CC and CCl neurons are not

included in the Cre-expressing population. The magnitude of partial expression in CT neurons was then determined from bead-uptake and immunohistochemistry for the genetic marker Forkhead box protein P2 (FoxP2).

The physiological function of CT neurons remains unclear but it has been suggested that they could provide a variable gain control for the transfer of sensory information regulated by attention and state of arousal (Ahlsén, Lindström, & Lo, 1985; Granseth, 2004). The selective expression of Cre-recombinase in CT neurons in layer 6 provides us with the opportunity to investigate the effects of acetylcholine, a neurotransmitter with an established role in both attention and arousal, in a more targeted manner than previously possible (Guillem et al., 2011; Lambe, Picciotto, & Aghajanian, 2003; Steriade, 2004). We find that muscarinic and nicotinic acetylcholine receptors increase excitability by depolarizing CT neurons. This demonstrates that acetylcholine can directly recruit this cell type during changes in attentional demand or arousal.

2 | MATERIAL AND METHODS

2.1 | Animals

Mouse lines were obtained from The Jackson Laboratory, USA. **Ntsr1-tdTom** mice, a cross between (B6.FVB(Cg)-Tg(Ntsr1-cre) GN220Gsat/Mmcd, RRID: MMRRC_030648-UCD) × (B6.Cg-Gt (ROSA)26Sor$^{tm14(CAG-tdTomato)Hze}$/J, https://www.jax.org/strain/007914), were heterozygous for both alleles. Parvalbumin-positive interneurons in layer 6 were identified using mice heterozygous for **GAD67-EGFP** (CB6-Tg(Gad1-EGFP)G42Zjh/J, https://www.jax.org/strain/007677). All methods and procedures were approved by the Linköping Committee for the Ethical Use of Animals in Research according to Swedish and EU laws and regulations.

2.2 | Electrophysiology

Coronal slices containing V1 were prepared from Ntsr1-tdTom or GAD67-EGFP mice. Mice, 3–8 weeks old of either sex, were deeply anaesthetized with isofluorane and decapitated. Brains were quickly submerged in ice-cold storage artificial Cerebral Spinal Fluid (storage-aCSF in mM: NaCl 124, $NaHCO_3$ 26, KCl 3, NaH_2PO_4 1.25, Myo-inositol 3, $MgCl_2$ 2, Lactic acid 4 and Ascorbic acid 0.5) equilibrated with 95% O_2 and 5% CO_2. V1 was cut in 400 μm coronal sections with a VT1200 vibratome (Leica Biosystems) while bathed with cold sucrose-aCSF (in mM; sucrose 248, D-Glucose 10, $CaCl_2$ 0.5, $NaHCO_3$ 26, NaH_2PO_4 1.25, $MgCl_2$ 6, KCl 3, Lactic acid 4, Myo-inositol 3 and Ascorbic acid 0.5) equilibrated with 95% O_2 and 5% CO_2. Sections were transferred to storage-aCSF and incubated at 37°C for 1 hr. Subsequent storage of slices was at room temperature.

During whole-cell recordings, slices were perfused with recording-aCSF (in mM; NaCl 126, $NaHCO_3$ 26, NaH_2PO_4 1.25, KCl 3.5, $MgSO_4$ 1, $CaCl_2$ 1.0 and D-glucose 10), bubbled with 95% O_2 and 5% CO_2, at 36°C. Data was recorded with a Multiclamp 700B amplifier (Axon instruments), filtered at 5 kHz and digitized at 16-bit depth at 10 kHz sample rate with Digidata 1440 (Axon Instruments).

Current-clamp recordings were made with a K-gluconate based pipette solution (in mM; K-gluconate 120, KCl 20, NaCl 5, phosphocreatine 10, HEPES 10, Mg-ATP 2, Na-GTP 0.3) adjusted with KOH to pH 7.3 and with an osmolarity of 290 mOsm. Micropipettes were pulled from borosilicate glass using a heated-filament vertical puller (Heka Elektronik). Micropipette tip resistance was of 6–9 MΩ. A fluorescence and IR-DIC microscope with a 0.8 NA 40× water immersion objective (Carl Zeiss) was used for visualizing neurons. Fluorescent labels were detected with appropriate filter-sets and excited by LEDs (Carl Zeiss). An Alexa488- or 594-conjugated dextran (Life Technologies) was included in the internal solution for confirmation of cell morphology during the recording session, Neurobiotin (Life Technologies) was also included for post-fixation neuronal reconstructions. All drugs used in this study were bath applied. Drugs were only applied once to each slice to avoid putative effects from receptor desensitization. The following drugs were supplied by Tocris: DL-2-Amino-5-phosphonopentanoic acid (APV), Carbamylcholine (Carbachol, CCh), Mecamylamine (MMA) and Muscarine iodide. The following drugs were supplied by Alomone labs: 6,7-Dinitroquinoxaline-2,3-dione disodium (DNQX), 10,10-bis(4-Pyridinylmethyl)-9 (10H)-anthracenone dichloride (XE991) and Tetrodotoxin (TTX). Tetraethylammonium chloride (TEA) was supplied by Sigma.

Data was analyzed using IgorPro (WaveMetrics Inc.). For the analysis of V_m and input resistance (R_i), current clamp protocols had test pulses (−50 pA for 500 ms) repeated every 20 s. TTX had no significant effect on resting V_m or R_i in either CT neurons ($n = 34$) or FS interneurons ($n = 7$). Cellular $\%R_i$ was calculated as ratios between the R_i after and before addition of drugs (R_i/R_{i0}-1 (%)). In order to evaluate the change in action potential frequency we calculated the average frequency during the initial (BL_i) and final (BL_f) minute of baseline, and the last minute of drug exposure. Baseline variability was calculated as $((BL_f - BL_i)/BL_i)$.

After electrophysiology, slices with biotin-filled cells were fixed overnight in 4% paraformaldehyde in PBS (pH 7.4), permeabilized in PBS with 1% Triton-X100 (PBS-T) followed by blocking solution (20% donkey serum in PBS-T). Slices were washed and incubated in Alexa488-conjugated streptavidin (Life Technologies) at 5 μg/mL in PBS-T with 1% donkey serum at 4°C. After 24 hr incubation, slices were washed three times in PBS and mounted onto glass slides with Vectashield hard-set mounting medium (Vector Laboratories).

2.3 | Anatomical tracing

Stereotaxic injections of fluorescein-conjugated RetroBeads™ (Lumafluor Inc.) were made into the lateral geniculate nucleus (dLGN, relative to Bregma: anterioposterior −2.5 mm, mediolateral ±2.1 mm and dorsoventral −3.2 mm) or claustrum (relative to Bregma: anterioposterior +0.14 mm, mediolateral −3.11 mm and, dorsoventral −4.0 mm) of adult Ntsr1-tdTom mice of either sex. Animals were anaesthetized with isofluorane supplemented with a local anesthetic. A Hamilton syringe was inserted through a hole drilled in the skull and 0.5 μl of retrobeads was injected over 10 min, with a post-injection resting period of 3 min before syringe retraction. Mice were sacrificed 7 days post-injection using CO_2, and transcardially perfused with PBS (pH 7.4)

TABLE 1 Antibodies used in the manuscript

Antibody name	Immunogen	Manufacturer catalog #	Concentration used
Anti-GFP[a] antibody	Recombinant GFP made in *E. coli*.	Aves labs. Chicken polyclonal. Catalog number: GFP-1020. LOT number: 0511FP12. RRID: AB_10000240	Diluted 1:1,000 (10 μg/mL) in PBS (0.1% Triton X-100 and 1:100 of BlokHen)
Anti- FoxP2[b] antibody	Synthetic peptide derived from within residues 700 to the C-terminus of Human FoxP2 conjugated to KLH[c]	Abcam. Rabbit polyclonal. Catalog number: ab16046. LOT number: GR191926-1. RRID: AB_2107107	Diluted 1:2000 (0.5 μg/ml) in BioSite Histo antibody diluent.

[a]Green fluorescent protein.
[b]Forkhead box P2.
[c]Keyhole limpet hemocyanine.

followed by 4% paraformaldehyde in PBS (pH 7.4). Brains were post-fixed for 4 hr, washed and stored in PBS at 4°C. Coronal or sagittal sections, 50 μm, were cut on a VT1200 vibratome (Leica). Sections were mounted with Vectashield hard-set.

2.4 | tdTomato intensity

Sections for tdTomato intensity profiles were prepared from paraformaldehyde fixed Ntsr1-tdTom mice, as above. Ntsr1-tdTom mice of three different ages were used; post-natal day 1 (d1); 5 week (5w) and 24 week (24w) old. All sections were mounted on glass slides and d1 sections were additionally stained with Draq7 (424001 BioLegend) to visualize cell nuclei. All slides were mounted with Vectashield hard-set.

2.5 | Immunohistochemistry

Sections for GFP or FoxP2 antibody staining were prepared from perfusion-fixed GAD67-EGFP or Ntsr1-tdTom mice, respectively, as above. For GFP staining, sections were permeabilized in PBS-T then transferred to Blokhen blocking solution (Aves Labs Inc, BH-1001) and incubated with chicken anti-GFP antibody (Aves Labs Inc, GFP-1020, RRID: AB_10000240), 1:1,000 for 24 hr. Sections were washed with PBS-T, then incubated with Fluorescein-conjugated goat anti-chicken secondary antibody (Aves Labs Inc, F-1005, RRID: AB_2313516) for 24 hr, then washed and mounted. For FoxP2 staining, sections were mounted on glass slides and antigenic retrieval was performed with pH 9 Tris-EDTA at 80°C for 2 min, slides were then permeabilized and washed in Tris-buffered saline (TBS) with 1% Tween (Nordic Biosite). Slides were incubated overnight with a polyclonal rabbit FoxP2 antibody, 1:2,000 (Abcam ab16046, RRID: AB_2107107) in BioSite Histo antibody diluent (BCB-20005, Nordic BioSite). Slides were washed in TBS-Tween and incubated with Alexa488-conjugated goat anti-rabbit secondary antibody (Life Technologies, A11008) for 1 hr. After staining, slides were washed in TBS-tween followed by PBS and then mounted with Vectashield hard-set. See Table 1 for a summary of the antibodies that were used.

2.6 | Antibody characterization

Previous studies have performed western blots on rodent brain extracts detecting a band of the right size as FoxP2 (Bowers, Perez-Pouchoulen, Roby, Ryan, & McCarthy, 2014; Hu et al., 2009). Our FoxP2 antibody staining was also comparable to the pattern observed with in situ hybridization (ISH) data from the Allen Brain Institute (brain-map.org). Controls omitting primary antibody did not show any nonspecific nuclear staining in our visual cortex sections. We used an anti-GFP antibody to amplify faded GFP staining. The EGFP-expression from unfixed sections matched the staining pattern from our GFP antibody staining. Further, the GFP antibody-staining pattern matched the appropriate pattern of cellular morphology and distribution as demonstrated previously by Chattopadhyaya et al. (2004).

2.7 | Microscopy

Confocal image stacks (16-bit) were obtained with a LSM Zeiss 700B confocal microscope using a 0.8 NA 20× objective or 1.3 NA 40× oil IR-DIC objective (Carl Zeiss). Ntsr1-tdTom co-localization with either retrobeads or FoxP2 immunohistochemistry was analyzed in individual neurons for which the entire soma was present in the image stack. Recorded neurons were reconstructed from maximum intensity Z-projections of the image-stack using the NeuronJ (RRID: SCR_002074) plug-in (Meijering et al., 2004) for ImageJ (Schneider, Rasband, & Eliceiri, 2012).

2.8 | Statistics

Values are given as mean ± standard error of the mean (SEM) unless stated otherwise. Two-tailed Mann-Whitney tests were used for two-group comparisons. Kruskal-Walllis with a Dunn's post-test was used for multiple comparisons between groups. Wilcoxon's signed-ranks test was used for paired non-parametric comparisons. $p < .05$ was considered statistically significant.

3 | RESULTS

3.1 | Ntsr1-tdTom expression is specific for CT neurons

Crossing the GN220 mouse with a genetically modified mouse carrying a floxed gene for tdTomato (cross abbreviated as Ntsr1-tdTom) made it possible to identify Cre-expressing cells using fluorescence microscopy. From this cross, we see that pyramidal neurons in cortical layer 6 of many neocortical areas, including V1, express Cre-driven tdTomato (Figure 1a) (Gong et al., 2007; Kim et al., 2014; Olsen et al., 2012).

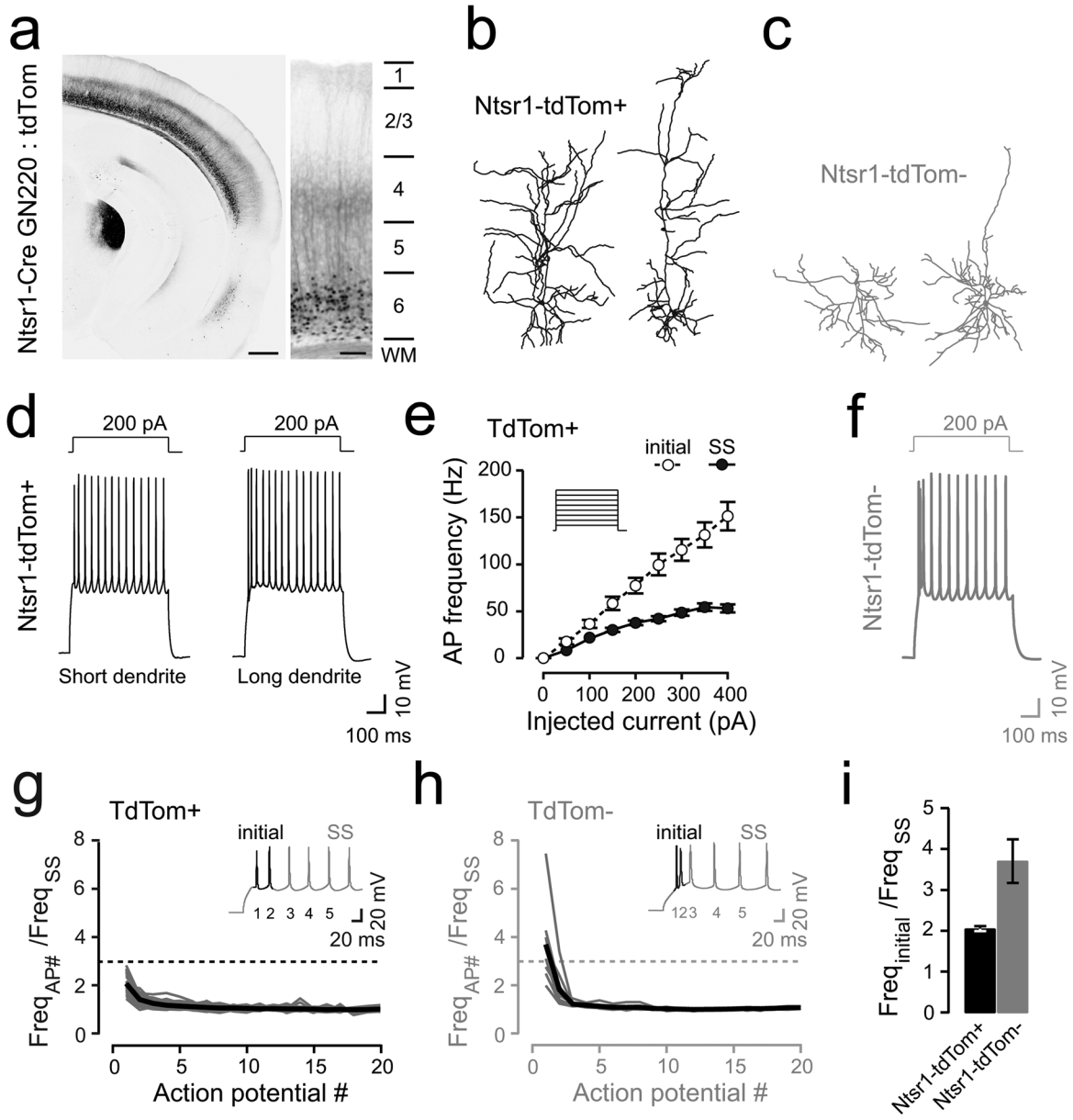

FIGURE 1 Action potential firing pattern and morphology of Ntsr1-Cre-positive neurons in layer 6 of V1 indicates that cells are CT neurons. (a) tdTomato-expression in a Ntsr1-tdTom mouse (inverted intensity confocal micrographs). Left is a coronal overview showing Ntsr1-tdTom-positive neurons in neocortical layer 6 and intense labeling of terminals in dLGN. Right is a magnification of V1 with cortical layering indicated to the right. tdTomato somata are localized to layer 6 while dendritic arborizations are seen throughout L5 and 4. A small proportion of dendrites continue past L4. Scale bar, 500 μm (left) and 100 μm (right). (b) Reconstruction of two neurobiotin-filled Ntsr1-tdTom-positive neurons, one with dendrite terminating in L4 (left) and one with dendrite extending to L1 (right). (c) Reconstruction of two neurobiotin-filled Ntsr1-tdTom-negative neurons, one inverted pyramid (left) and one pyramidal (right). (d) Action potential response to square depolarizing current of two Ntsr1-tdTom-positive neurons, one with dendrite extending to L4 (left) and one with dendrite extending to L1 (right). (e) Summary plot of action potential firing frequency versus injected current of Ntsr1-tdTom-positive neurons. Initial (dashed) and steady-state (solid) firing rates plotted separately. (f) Action potential response to square depolarizing current of a Ntsr1-tdTom-negative neuron. (g) Ratios of instantaneous action potential frequency over steady-state (SS) action potential frequency ($Freq_{AP\#}/Freq_{SS}$) of Ntsr1-tdTom-positive neurons ($n = 33$), individual cell recordings (grey) and mean (black). Dotted line indicates ratio 3. Inset, an example trace of square depolarizing current at 200 pA. (h) Plot of Ntsr1-tdTom-negative neurons ($n = 9$, data plotted as in g). (i) Bar graph for the ratio between the first two action potential firing frequency (initial) over the steady state, Ntsr1-tdTom-positive neurons (black, $n = 33$) and Ntsr1-tdTom-negative neurons (grey, $n = 9$). Data plotted as means ± *SEM*. Ntsr1, Neurotensin receptor 1; tdTom+, tdTomato positive; tdTom-, td Tomato negative; Freq, instantaneous action potential firing frequency; and SS, steady-state

As a first step toward identifying the type of pyramidal neuron labeled in the Ntsr1-tdTom mouse, we performed electrophysiological recordings. CT, and CC neurons differ with respect to their electrophysiological properties (Brumberg, Hamzei-Sichani, & Yuste, 2003; Mercer et al., 2005; Thomson, 2010; Velez-Fort et al., 2014). To assess the electrophysiological properties of Ntsr1-tdTom-positive neurons in layer 6, we prepared acute coronal slices from V1 and performed whole-cell patch-clamp recordings on fluorescent neurons. Injection of depolarizing current pulses above rheobase produced repetitive action potential firing (Figure 1d). The first two action potentials were in rapid succession (77.3 ± 8.2 Hz at 200 pA current injection) while later action potentials proceeded at about half that frequency (37.6 ± 2.5 Hz) with negligible adaptation (Figure 1e, g). This is the signature firing-pattern of CT neurons (Brumberg et al., 2003; Mercer et al., 2005).

The phasic/rapidly-adapting action potential response, typical of CC neurons (Brumberg et al., 2003; Mercer et al., 2005; Thomson, 2010) was not seen in recordings from Ntsr1-tdTom-positive neurons (Figure 1g). Neurobiotin was included in the intracellular buffer so that anatomical reconstructions could be made following the recordings. Reconstructions revealed that none of the Ntsr1-Cre-positive neurons had morphological traits characteristic of CC neurons, such as atypical apical dendrites (inverted or laterally extending). In recordings from Ntsr1-Cre-negative neurons in layer 6, the action potential responses to square depolarizing pulses were more varied (Figure 1h). In 5 out of 9 cells the instantaneous action potential frequency of the first pair of action potentials was >3 times the steady state firing rate, suggesting that the CC neurons belongs to the Cre-negative population in layer 6 of the Ntsr1-Cre GN220 mouse (Brumberg et al., 2003; Mercer et al., 2005; Thomson, 2010). Confocal microscopy of Ntsr1-tdTom-negative cells revealed pyramidal neurons with atypical dendrites (Figure 1c). Taken together, our morphological and electrophysiological characterization suggests that fluorescent cells in Ntsr1-tdTom mice are not CC neurons.

Confocal microscopy of the neurobiotin labeling in Ntsr1-tdTom-positive neurons revealed that the majority of recordings were made from pyramidal neurons with an apical dendrite that ended in a tuft in layer 4 (21 of 29; 72%; Figure 1b), as is characteristic of CT neurons (Cotel, Apergis-Schoute, & Williams, 2014; Thomson, 2010). However, in 8 out of 29 cells (28%) the apical dendrite extended to layer 1 (Figure 1b), a feature typically associated with CCl neurons. To distinguish between CT and CCl neurons we injected retrobeads into the dLGN or claustrum of Ntsr1-tdTom mice (Figure 2).

Following dLGN injections, retrograde labeling of neurons in primary visual cortex would serve as unambiguous identification of CT neurons. We found that 88.2 ± 3.8% of cells expressing Ntsr1-tdTom took up retrobeads from the dLGN (Figure 2c, d; $n = 690$ neurons from three mice). Occasional Ntsr1-tdTom-negative neurons containing retrobeads were detected, but typically retrobead-labeled neurons in layer 6 also expressed Cre-induced tdTomato (87.0 ± 3.3%, Figure 2d). These findings indicate that CT neurons are the predominant Cre-expressing neocortical cell type in the Ntsr1-Cre GN220 mouse. However, the roughly 10% of Ntsr1-tdTom-positive neurons that did not take-up retrobeads could indicate that a small population of non-CT neurons, presumably

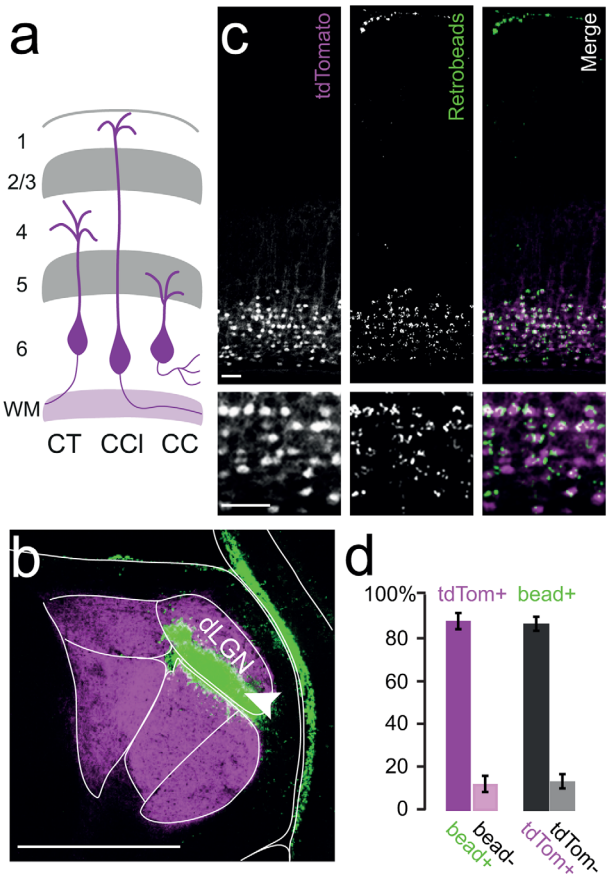

FIGURE 2 Retrobeads injected to dLGN show that Cre-expressing neurons in Ntsr1-Cre mice are CT neurons. (a) Schematic diagram depicting the three types of pyramidal neurons (CT, CCl, and CC) in layer 6. (b) Stereotaxic injection of retrobeads into the dLGN. Example dLGN retrobead injection site (arrow head), tdTomato and retrobeads. Scale bar, 400 μm. (c) Confocal images of V1 (above) and layer 6 magnification (below) following injection of retrobeads into dLGN. Scale bar, 50 μm. (d) Summary data describing the co-localization of tdTomato-positive and dLGN-retrobead-labeled neurons in V1. 88.2 ± 3.8% of tdTomato-positive neurons were labeled with retrobeads ($n = 690$ neurons, 3 mice) and 87.0 ± 3.3% of retrobead-labeled neurons were tdTomato-positive ($n = 695$ neurons, three mice). Data plotted as means ± *SEM*. dLGN, dorsolateral geniculate nucleus; Ntsr1, Neurotensin receptor 1; CT, corticothalmic; CCl, corticoclaustral and CC, corticocortical [Color figure can be viewed at wileyonlinelibrary.com]

CCl neurons, also express Cre. An alternative explanation could be that the dLGN injections fail to label every CT neuron in the neocortex.

We investigated if CCl neurons are Cre-positive by injecting retrobeads into the claustrum and searched for co-labeling of Ntsr1-tdTom-positive neurons in layer 6 (Figure 3a). In sagittal sections from the ipsilateral hemisphere, we observed multiple retrobead-labeled neurons in layer 6 of visual and somatosensory cortical areas, but none of these neurons expressed tdTomato (Figure 3a, b; $n = 34$ neurons in three mice). Thus, the Ntsr1-tdTom-positive neurons, even though they can have long apical dendrites, are unlikely to be CCl neurons. The likely reason that dLGN injections failed to label all Cre-positive neurons thus seems to be that some CT neurons fail to take up the marker.

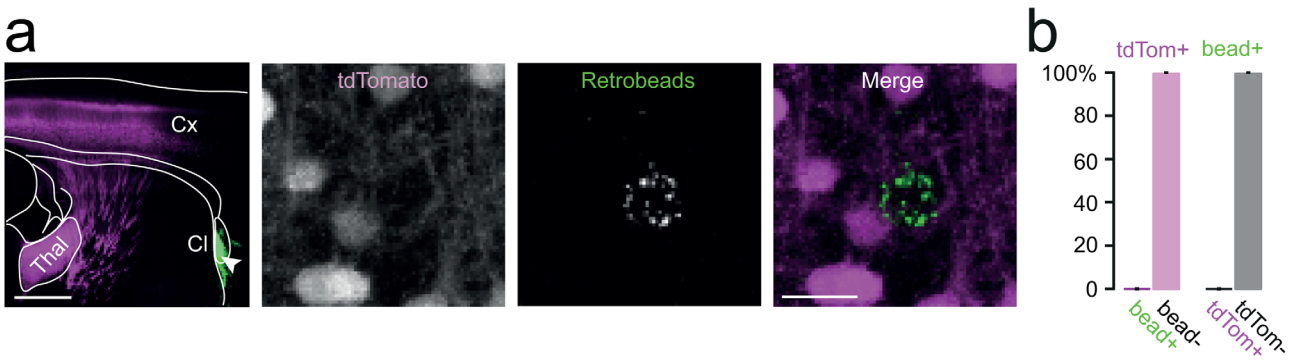

FIGURE 3 Retrobeads injected to Claustrum show that Cre-expressing neurons in Ntsr1-Cre mice are not CCl neurons. (a) Stereotaxic injection of retrobeads into the Claustrum (Cl). Left, sagittal view of Cl retrobead injection site (arrow head), tdTomato and retrobeads. Scale bar, 1000 μm. Remaining images are confocal micrographs visualizing a retrobead-labeled neuron in layer 6 of V1 that does not express tdTomato. Scale bar, 20 μm. (b) Summary data of Cl retrobead injections. Layer 6 neurons that project to Cl, identified by retrobead labeling, were never tdTomato-positive in Ntsr1-tdTom mice (100 ± 0%, $n = 34$ layer 6 neurons, three mice) and no tdTomato-positive neuron contained retrobeads (0 ± 0%, n = 1,654 layer 6 neurons, three mice). Data plotted as means ± *SEM*. Ntsr1, Neurotensin receptor 1; CCl, corticoclaustral; Cl, claustrum; Cx, cortex and Thal, thalamus [Color figure can be viewed at wileyonlinelibrary.com]

An alternative explanation for the presence of long apical dendrites in the Ntsr1-tdTom-positive neurons could be related to the sequence of changes in CT neuron dendritic morphology that occur during development. Pyramidal neurons in layer 6 of the mouse medial prefrontal cortex have apical dendrites that initially extend to layer 1, but then retract to layer 4 during development (Bailey, Alves, Nashmi, De Biasi, & Lambe, 2012). Whether the same is true of pyramidal neurons in layer 6 of the mouse visual cortex remains unknown. To examine developmental changes in apical dendrite extension across the population of Ntsr1-tdTom-positive neurons, we estimated the proportion of long versus short apical dendrites in mice at different ages using an optical sampling technique. Specifically, we compared the average fluorescence intensity in layer 2/3 to that in layer 5 (Figure 4). Since these regions are dominated by apical dendrite shafts, rather than dendritic tufts or axonal arborizations, their fluorescence intensity provides an estimate of the proportion of Ntsr1-tdTom-positive neurons with long relative to short apical dendrites. This estimate was similar between adult mice (week 24; 27.9 ± 3.02%, $n = 3$ mice) and young mice (week 5; 24.7 ± 4.56%, $n = 3$ mice). However, in newborn mouse pups (day 1) this estimate was significantly higher (68.9 ± 1.56%, $n = 3$) suggesting that apical dendrites more frequently extended to layer 1 early in development. This supports the notion that Ntsr1-tdTom-positive neurons initially have long apical dendrites that retract to layer 4 during development. However, it is clear from our adult samples that a significant proportion maintain this "immature" morphology long into adulthood, and significantly later than the time point at which we performed electrophysiological recordings.

3.2 | Partial expression of Cre recombinase in CT neurons

The histological and electrophysiological analyses show that Ntsr1-tdTom-positive neurons in the Ntsr1-Cre GN220 mouse are CT neurons. As Cre-expression is confined to a specific type of neurons we sought to investigate to what extent incomplete penetrance will lead to some CT neurons not expressing Cre. The finding that 13 ± 3.3% of the cells that took up beads from the dLGN were Ntsr1-tdTom-negative suggests that partial Cre-expression occurs (Figure 2d). We compared Cre-expression with a cell-type-specific immunohistochemical marker as an independent and complementing test for partial expression. The nuclear transcription factor Forkhead box protein P2 (FoxP2) defines a distinct sub-population of pyramidal neurons in layer 6 (Hisaoka, Nakamura, Senba, & Morikawa, 2010). Although the identity of this population has not been completely established, there are indications that they are CT neurons. We found that effectively all Ntsr1-tdTom-positive cells were FoxP2 positive in immunohistochemical stains of sections of visual cortex (98.3 ± 0.3%, $n = 775$ neurons from 4 mice; Figure 5). That Ntsr1-tdTom-expression is completely confined to the FoxP2 expressing population in neocortical layer 6 further strengthens the indication that FoxP2 expressing cells are CT neurons indeed. The small proportion of FoxP2 positive cells that do not express Ntsr1-tdTom then provides a measurement of the extent of partial expression of Cre in CT neurons in the GN220 Ntsr1-Cre mouse line: 9.3 ± 2.3% ($n = 828$ cells from 4 mice; Figure 5). This is the most likely conclusion, but we cannot entirely exclude the possibility that these cells constitute a separate FoxP2 subpopulation of non-CT neurons that coincidentally match the size of a Cre-negative-bead-positive CT population.

3.3 | Cholinergic pathways can directly affect CT neurons

Having established that Ntsr1-tdTom-positive neurons are CT neurons, we chose to demonstrate how this tool could be used to clarify signaling pathways within the complex network of cortical layer 6. Since CT neurons have been suggested to have a role in attention and arousal they are a relevant target for cholinergic signaling; however, it is not known if CT neurons can directly respond to cholinergic modulation.

To determine if cholinergic modulation occurs at CT neurons we applied acetylcholine (ACh), to the extracellular buffer during whole-

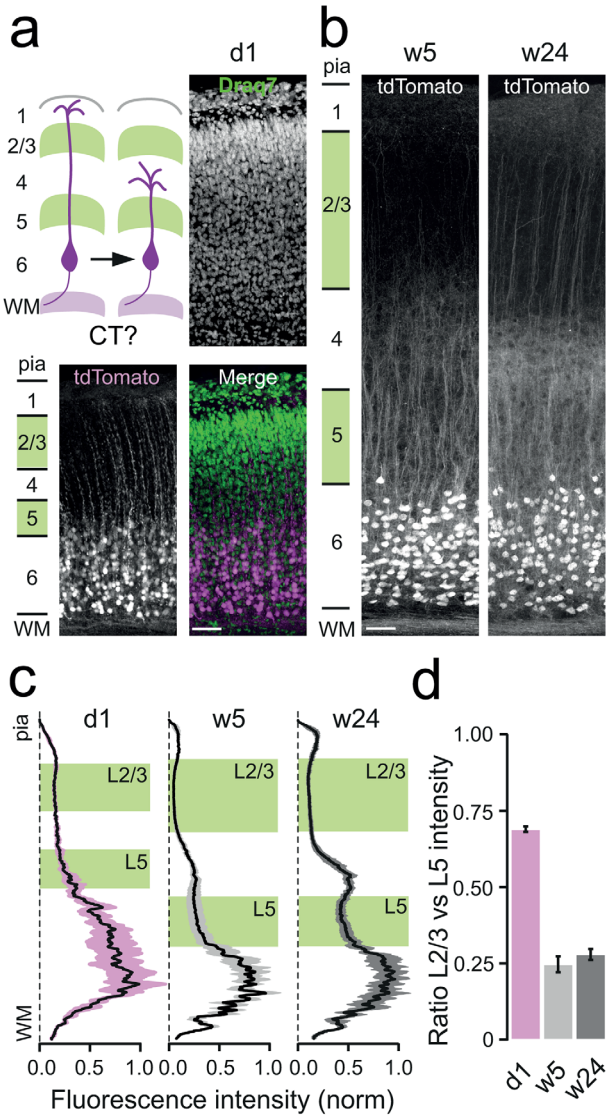

FIGURE 4 The majority of Ntsr1-tdTom-positive neurons retract their apical dendrite from layer 1 to layer 4 during development. (a) Top left, Schematic diagram illustrating developmental retraction of the apical dendrite. Confocal micrographs show tdTomato expression in visual cortex from a postnatal day 1 (d1) Ntsr1-tdTom mouse. The nuclear marker Draq7 was used to identify the different layers, as indicated to the left. Apical dendrites project to superficial layers. Scale bar, 50 μm. **b**, Confocal micrographs from 5-week-old (w5) and 24-week-old (w24) Ntsr1-tdTom mice reveal a reduction in tdTomato-positive apical dendrites in the superficial layers, layers indicated as in (a). Scale bar, 50 μm. (c) Average tdTomato fluorescence intensity profiles across cortical layers for d1 ($n = 3$), w5 ($n = 3$) and w24 ($n = 3$) mice. Shaded regions indicate the portions of the intensity profiles that were used to estimate the ratio of long (crossing L2/3) relative to short (crossing L5) apical dendrites. (d) Summary of the ratio between long and short apical dendrites in the three age groups. The ratio was calculated by dividing the average fluorescence across L2/3 by that from L5. In newborn mice, most apical dendrites appear to be long, while the proportion is lower at w5 and w24. Data plotted as means ± *SEM*. Ntsr1, Neurotensin receptor 1; L2/3 & L5, layer 2/3 and 5; WM, white matter [Color figure can be viewed at wileyonlinelibrary.com]

cell recordings in slices from V1 (4–8-week-old Ntsr1-tdTom mice). We used a concentration of ACh (100 nM) similar to levels previously measured in vivo with microdialysis (Vinson & Justice, 1997). ACh produced a notable increase in the instantaneous action potential firing rate of Ntsr1-tdTom-positive CT neurons (3.5 ± 0.6 Hz before to 6.0 ± 1.3 Hz after exposure). The ACh-induced increase in firing (73.7 ± 24.4%) was significantly different from baseline variability (−0.6 ± 6.6%; $p = .02$ Wilcoxon signed rank test; $n = 9$; Figure 6a, b). ACh did not evoke any significant change in membrane potential (V_m) compared to baseline (−59.5 ± 2.4 mV baseline and −57.2 ± 3.4 mV ACh; $p = .5$; $n = 8$), although the exact membrane potential is obscured by action potential firing. However, ACh generated a significant increase in input resistance (R_i) compared to baseline (376 ± 87.6 MOhm before and 425 ± 89.7 MOhm after ACh; $p = .008$; $n = 8$).

To determine if the ACh-mediated increase in CT neuron firing rate resulted from a direct effect on CT neurons or was inherited from other excitatory neurons in the cortical network, we blocked glutamatergic neurotransmission with 20 μM DNQX and 100 μM APV. Following glutamate block, 100 nM ACh still produced an appreciable increase in the instantaneous action potential firing rate from 3.2 ± 0.6 Hz to 4.8 ± 1.2 Hz. This increase (45.2 ± 14.9%) was significantly greater than baseline variability (3.7 ± 11.3%, $p = .05$ Wilcoxon signed rank test; $n = 6$; Figure 6b). This result demonstrates that ACh does not require an intact excitatory network to increase Ntsr1-tdTom-positive neuron firing.

To further study the nature of cholinergic signaling at CT neurons we blocked all network activity in the slice preparation using tetrodotoxin (TTX, 0.5 μM). We also increased the sensitivity for detection of cholinergic effects by using the cholinesterase-resistant cholinergic agonist carbamylcholine (Carbachol, CCh) at a concentration (50 μM) sufficient to saturate muscarinic (m)AChR-binding. Additionally, parvalbumin-positive fast-spiking (FS) interneurons (Figure 6e), a cell type known to show no or little responses to CCh (Gulledge, Park, Kawaguchi, & Stuart, 2007; Xiang, Huguenard, & Prince, 1998), were used as a comparison for the CCh-sensitivity of Ntsr1-tdTom-positive neurons.

Under control conditions, the V_m of CT neurons (−62.4 ± 1.2 mV; Figure 6c, d) and FS interneurons (−62.6 ± 1.5 mV; Figure 6f) were similar. However, the effect of CCh was noticeably different. FS interneurons showed a small but significant change in V_m (−56.2 ±2.9 mV with CCh, $p = .04$, $n = 7$) but with no significant change in average input resistance (R_i; 194 ± 36.8 MOhm control vs. 204 ± 36.4 MOhm CCh, $p = .78$, $n = 7$). In contrast, CCh application produced a strong V_m depolarization (to −44.7 ± 2.6 mV, $p < .0001$, $n = 15$), and increased the R_i (from 211 ± 15.6 MOhm to 287 ± 25.6 MOhm, $p = .03$, $n = 15$) of CT neurons. Since these experiments were done in the presence of TTX, these changes in V_m and R_i confirm that the observed cholinergic modulation of CT neurons is mediated by a direct mechanism.

To differentiate between mAChR and nAChR activation we performed experiments using agonists and antagonists that specifically target either type of receptor. During wash-in of CCh, a fast but transient depolarization followed by a sustained depolarization was observed in the V_m of CT neurons (Figure 7a). The transient component was absent

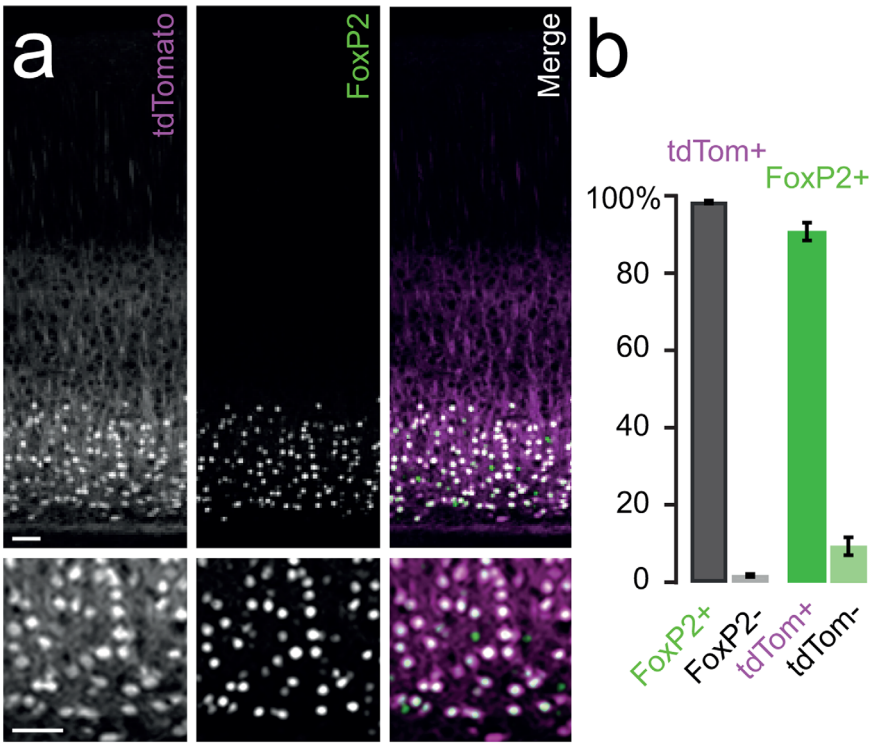

FIGURE 5 Ntsr1-tdTom-positive neurons immunolabel with antibodies against the layer 6 specific marker FoxP2. (a) Confocal images of V1 (above) and layer 6 (below) showing labeling for tdTomato, and FoxP2. Scale bar, 50 μm. (b) Summary plot of the co-localization between tdTomato-positive and FoxP2-immunostained neurons. 98.3 ± 0.3% of tdTomato-positive neurons stained positive for FoxP2 ($n = 775$ neurons, 4 mice) and 90.8 ± 2.3% of FoxP2 cells were tdTomato-positive ($n = 828$ neurons, 4 mice). Meaning that virtually all Cre-expressing neurons in layer 6 express FoxP2. Data plotted as means ± *SEM*. FoxP2, Forkhead box protein P2 [Color figure can be viewed at wileyonlinelibrary.com]

when muscarine (50 μM), a mAChR selective agonist, was used (Figure 7b). To investigate if nAChRs are responsible for the transient component, we pre-incubated V1 slices with the nAChR-antagonist Mecamylamine (MMA; 50 μM) before adding CCh (50 μM). MMA-pretreatment eliminated the transient depolarization (Figure 7c). In conclusion, both mAChRs and nAChRs depolarize CT neurons. When the cholinergic agonist is bath-applied nAChRs appear to be responsible for an initial transient depolarization, while mAChRs contribute to a sustained depolarization.

The increase in R_i observed during the carbachol-induced depolarization of CT neurons, suggests that mAChRs are inducing the closure of K^+ channels. Ntsr1-Cre-positive neurons express M_1 and M_3 type mAChRs (Tasic et al., 2016), which can mediate closure of M-type K^+ channels. Therefore, we applied the M-channel selective antagonist XE991 (10–25 μM) to the CT neurons. XE991 produced a small depolarization of V_m (ΔV_m 3.3 ± 0.9 mV with XE991 vs. 0.55 ± 0.4 mV control; $p = .03$, $n = 6$, Figure 8a, b) and an equally small, but non-significant, increase in R_i (ΔR_i 12.7 ± 8.2% with XE991 vs. 0.8 ± 2.1% control; $p = .47$, $n = 6$, Figure 8b), providing evidence that M-channels are open during basal conditions. Subsequent bath application of CCh produced an additional depolarization (ΔV_m 11.6 ± 3.9 mV, $p = .06$, $n = 6$) with an increase in R_i (ΔR_i 17.7 ± 5.9%, $p = .2$, $n = 6$; Figure 8b) but with a higher cell-to-cell variability than in recordings without XE991 the responses to CCh were non-significant. From this we conclude that closure of M-type K^+ channels cannot be the sole mechanism for cholinergic modulation of CT neurons.

We also determined the effect of the non-selective K^+ channel blocker, TEA (10 mM). When TEA was added, CT neurons depolarized by 5.6 ± 1.3 mV (vs. 0.9 ± 0.4 mV control; $p = .002$, $n = 6$; Figure 8c, d) with a concomitant increase in R_i (24.1 ± 5.7% vs. 1.04 ±0.8% control; $p = 0.004$, $n = 6$; Figure 8d). Subsequent bath-application of CCh had no appreciable effect on V_m ($p = .24$, $n = 6$) or R_i ($p = 0.79$, $n = 6$; Figure 8d). Since non-selective blockade of K^+ channels abolished the CT neuron response to CCh, it can be concluded that closure of K^+ channels was necessary for the observed CCh-induced depolarization. However, in addition to blocking K^+ channels, TEA also acts as a competitive antagonist to CCh at nAChRs (Akk & Steinbach, 2003). Thus, the complete block of the CCh-induced depolarization by TEA, seems to come from combined blockade of mAChR and nAChR in CT neurons (Figure 8e).

4 | DISCUSSION

Our results demonstrate that Ntsr1-Cre driven tdTomato-expressing cells in cortical layer 6 of the GN220 mouse comprise the population of pyramidal neurons that project to the thalamus (CT neurons) and not neurons projecting to the claustrum (CCl neurons) or terminating within the cortex (CC neurons). This conclusion is based on a

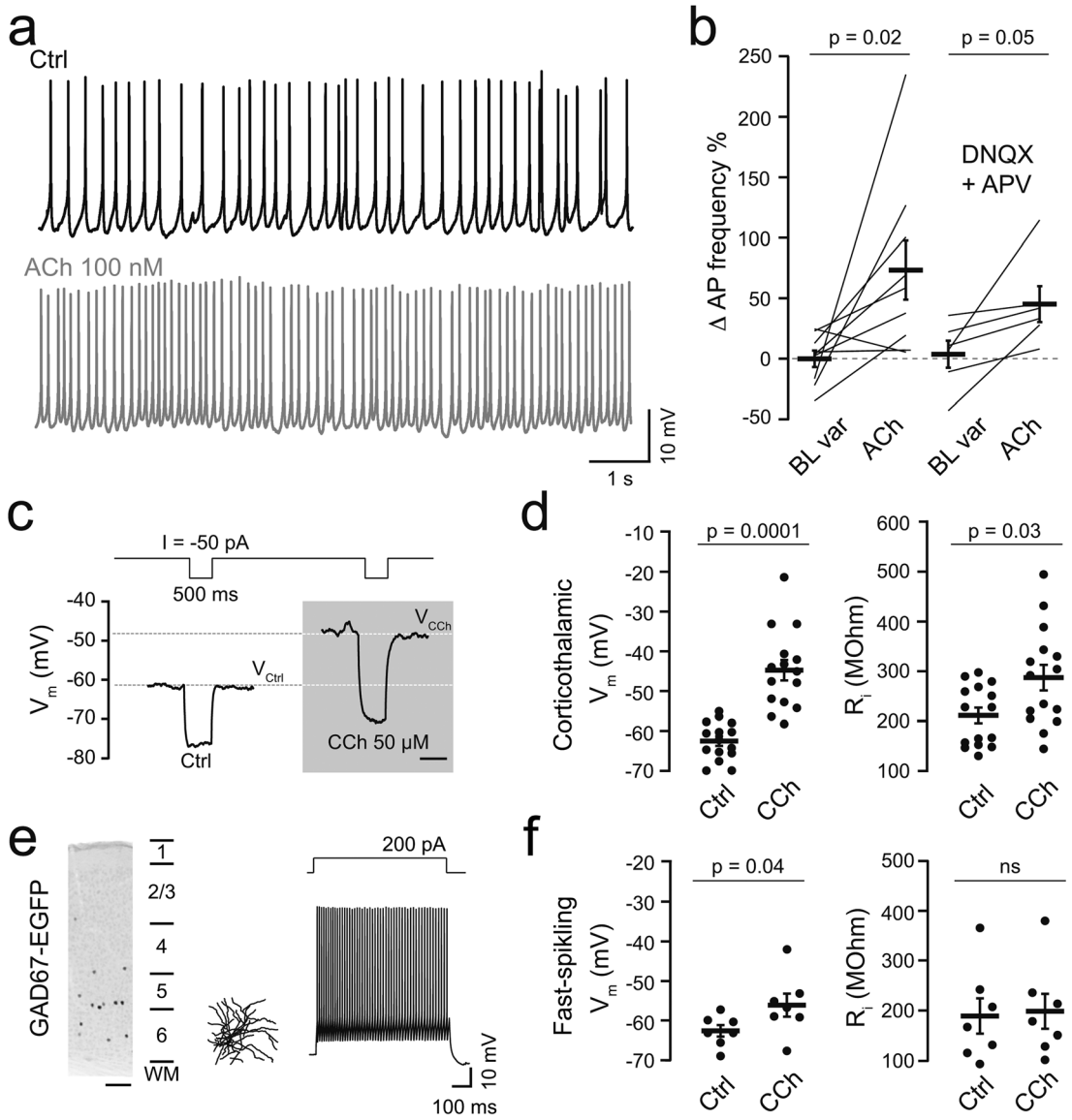

FIGURE 6 CT neurons increase action potential firing upon bath-application of a physiological concentration of Acetylcholine (ACh) and are depolarized by carbachol (CCh). (a) Sample trace from a representative CT neuron (black) that responded with increased action potential firing during bath-applied 100 nM ACh (grey). (b) Compared to baseline variability (BL var), action potential firing increased in most CT neurons when exposed to ACh (left; $-0.6 \pm 6.6\%$ BL var vs. $73 \pm 24.4\%$ ACh; $p < .05$; $n = 9$). This increase persisted in the presence of DNQX and APV (right; $3.7 \pm 11.3\%$ BL var vs. $45.2 \pm 14.9\%$ ACh; $p \leq .05$; $n = 6$). (c) 50 µM CCh generates a substantial depolarization of the resting membrane potential (V_m) and change in input resistance (R_i). Sample traces showing responses to test pulses (-50 pA for 500 ms) from a CT neuron before and after CCh application. Action potential firing blocked with TTX. Scale bar, 500 ms. (d) CT neurons significantly depolarized (left) and increased R_i (right) with CCh ($n = 15$; p values for Mann–Whitney test). (e) Antibody staining against EGFP in V1 of a GAD67-EGFP mouse (left). Reconstruction of a neurobiotin-filled EGFP-positive neuron (middle) and its response to square depolarizing current injection (right). All EGFP-positive neurons in layer 6 were of the fast-spiking (FS) type ($n = 7$). Scale bar, 100 µm. (f) In FS interneurons CCh had a small but significant effect on V_m (left) but not R_i (right) ($n = 7$; p values for Mann-Whitney test). Data plotted as means ± *SEM*. CT, corticothalamic; ACh, acetylcholine; BL var, baseline variability; AP, action potential; CCh, carbachol; TTX, tetrodotoxin; R_i, input resistance; FS, fast-spiking and V_m, membrane potential

combination of morphological and electrophysiological evidence. First, we demonstrated that Ntsr1-tdTom-positive neurons display a minimally adapting action potential firing pattern that is characteristic of CT neurons (Figure 1d, e, g). Second, similar to (Denman & Contreras, 2015) we observed dense projections of Ntsr1-tdTom-positive axons from cerebral cortex terminating in the thalamus (Figure 2b). Third, we found that the vast majority of Ntsr1-tdTom-positive pyramidal cells in V1 took up retrobeads injected to the dLGN (Figure 2c, d). Two previous studies report similar results after dLGN injections (Bortone, Olsen, & Scanziani, 2014; Kim et al., 2014); however, the proportion of Cre-expressing neurons that take up retrobeads varies between 100% (Bortone et al., 2014) and ~85% (our study & Kim et al., 2014). A likely

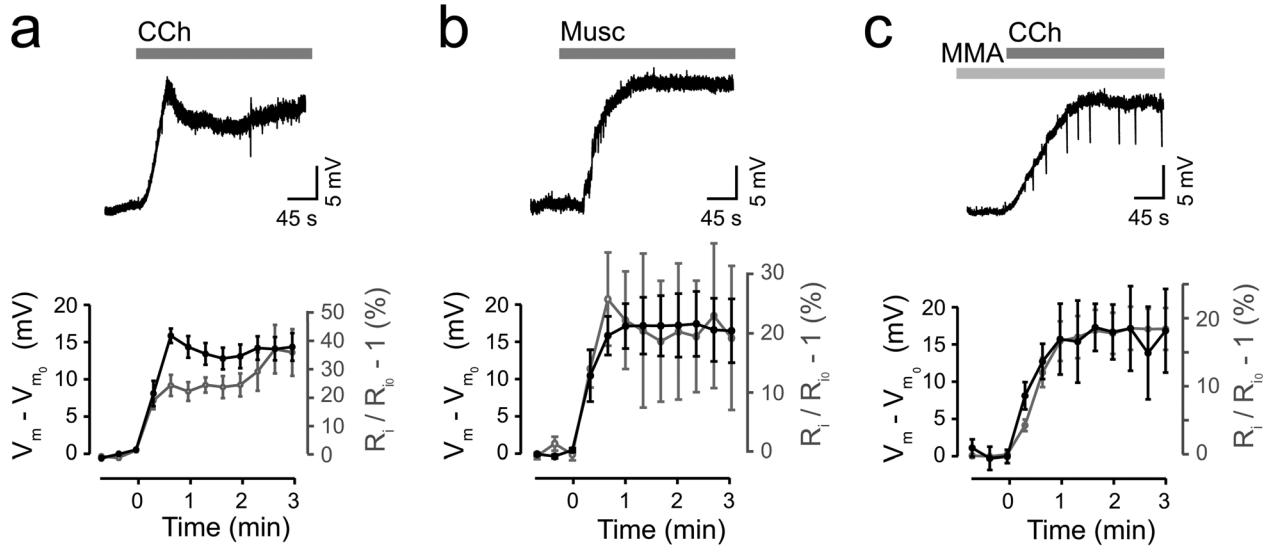

FIGURE 7 CT neurons are depolarized by CCh acting on both muscarinic and nicotinic acetylcholine receptors. (a) 50 μM Carbachol (CCh, grey bar) elicits a large depolarization, with transient and sustained components, in CT neurons. Top, Example trace showing CCh-evoked depolarization in a typical CT neuron. Bottom, Plot comparing changes in V_m (black, left axis) and R_i (grey, right axis) during CCh application. Time is relative to start of wash-in ($n = 9$ CT neurons). (b) 50 μM Muscarine (Musc, grey bar) elicits a large depolarization, without the transient component (plotted as in a), $n = 5$ CT neurons. (c) Following pre-incubation of 50 μM Mecamylamine (MMA), application of 50 μM CCh (grey bars) elicits a large depolarization, without the transient component (plotted as in a), $n = 7$ CT neurons. Data plotted as means ± *SEM*. CT, corticothalamic; V_m, membrane potential; R_i, input resistance; CCh, carbachol; Musc, muscarine and MMA, mecamylamine

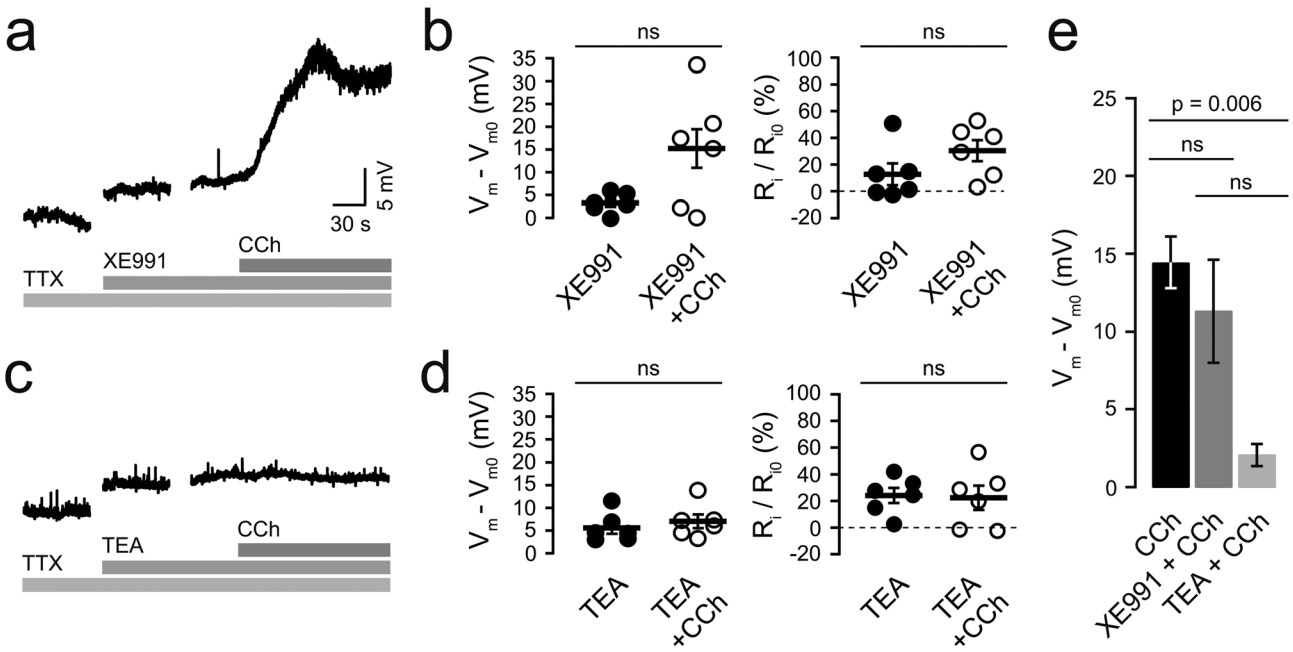

FIGURE 8 Tetraethylammonium (TEA) prevents the CCh induced depolarization in CT neurons. (a) Representative traces from a CT neuron showing the experimental paradigm for testing M-channel contribution to CCh response. Horizontal bars indicate application of specified drugs. (b) Plots of the change in membrane potential (left, ΔV_m relative to TTX) and input resistance (right, ΔR_i relative to TTX) produced by addition of the M-channel blocker XE991 and subsequently CCh. Note that XE991 alone produced a small but significant depolarization associated with a R_i increase that was not significant ($n = 6$ CT neurons Mann-Whitney test). Subsequent CCh-induced changes were not significant ($n = 6$; p from Mann-Whitney test). (c, d) Effect of non-selective K^+ channel blocker (TEA), plotted as in (a) and (b). In presence of TEA the CCh-induced depolarization was no longer present ($n = 6$, CT neurons). (e) Summary plot of the steady-state ΔV_m effect of CCh alone (black); in presence of XE991 (grey); or TEA (light grey). Values in e are changes relative to baseline with antagonist immediately before adding CCh. Data plotted as means ± *SEM*. TEA, tetraethylammonium; CCh, carbachol; CT, corticothalamic and TTX, tetrodotoxin

explanation for this discrepancy would be the size of injections, with higher co-labeling resulting from injections that encompass lateral dorsal and lateral posterior thalamic nuclei in addition to the dLGN.

We demonstrate that CC neurons do not express Cre-recombinase based on two pieces of evidence: First, recorded Ntsr1-tdTom-positive neurons never respond to square-pulse current injections with phasic/rapidly adapting (>3 times difference between first pair and steady-state, Figure 1g) action potential firing. Second, inverted and laterally extending pyramidal neurons were not observed during confocal imaging of recorded Ntsr1-tdTom-positive neurons. Both these features could be seen in Ntsr1-tdTom-negative neurons in layer 6 (Figure 1c, h).

While 24–28% of Ntsr1-tdTom-positive neurons have long apical dendrites, we conclude that they are likely not CCl neurons. This conclusion is based on the observation that all layer 6 neurons with uptake of retrobeads from the claustrum were Ntsr1-tdTom-negative (Figure 3b). Instead, we suggest that the long apical dendrites are a carry-over of "immature" CT morphology. We found that layer 6 CT neurons in visual cortex initially (day 1) have a long apical dendrite that retracts to layer 4 during development (Figure 4), as has been shown in prefrontal cortex (Bailey et al., 2012). Interestingly, a significant proportion of CT neurons maintain long apical dendrites until at least 24 weeks of age. This is in conflict with what has been found in other species (i.e., cat and rat), but it should be noted that other investigations in mice also encounter CT neurons with long apical dendrites (Velez-Fort et al., 2014). However, we cannot entirely exclude the possibility that Ntsr1-tdTom-positive neurons with long apical dendrites project to an unknown location (rather than the claustrum or thalamus, Briggs, 2010).

We show that FoxP2 co-localizes with tdTomato in V1 of Ntsr1-tdTom mice (Figure 5). This novel finding enables FoxP2 to be used as a marker of putative CT neurons in future studies. Our results with FoxP2 co-staining also provide an indication of the identity of retrobead-containing cells that were not Ntsr1-tdTom-positive. While essentially all Ntsr1-tdTom-positive neurons were immunopositive for FoxP2, 9.2% of FoxP2 neurons did not have tdTomato (Figure 5b). This number is comparable in magnitude to the 13% of neurons that take up retrobeads from the dLGN but lack Ntsr1-tdTom (Figure 2d). It seems as not all CT neurons express Cre. Given that the expression of the *NTSR1* gene is weak in layer 6 (Tasic et al., 2016) the partial expression of Cre-recombinase in CT neurons is not surprising. The proportion of neurons that do not express Cre-recombinase is minor, but needs to be considered when interpreting the results from studies using the Ntsr1-Cre mouse to target genetic tools for the stimulation or inhibition of CT neurons.

We find that CT neuronal activity is strongly modulated by cholinergic drugs. Traditionally it is thought that cholinergic neurons in the basal forebrain release acetylcholine within the neocortex via non-specific volume transmission (Descarries, Gisiger, & Steriade, 1997; Mrzljak, Pappy, Leranth, & Goldman-Rakic, 1995). We replicated this type of transmission in the slice preparation by adding a physiological concentration (100 nM) of ACh to the extracellular buffer and found that low levels of cholinergic modulation increased action potential firing of CT neurons (Figure 6a, b). This increase was partly mediated by direct depolarization of CT neurons. However, previously identified cholinergic effects on neurons and synapses upstream the CT neurons are also likely to contribute to the excitatory drive of this circuit (Guillem et al., 2011; Lambe et al., 2003). ACh is known to depolarize pyramidal neurons in other layers of cortex (Krnjević, Pumain, & Renaud, 1971; Thiele, 2013), and in the present study we firmly establish that this is also true of the CT neuron population. We show that both mAChRs and nAChRs on CT neurons contribute to this depolarization. Nicotinic AChRs have much lower affinity for ACh (and CCh) and faster desensitization compared to mAChR, making volume transmission (and our method for drug application) less than optimal for characterizing the nAChR component. Thus, we see the nicotinic component primarily early during wash-in of the cholinergic agonist. However, during physiological conditions, nAChRs are likely to function at synapses (Hay, Lambolez, & Tricoire, 2015; Hedrick & Waters, 2015) with roles quite different to the more generalized modulation from volume transmission. This dichotomy between the action of mAChRs and nAChRs on CT neurons could thus serve as the substrate for different levels of gain regulation by the CT pathway. More specifically, volume transmission acting through mAChRs would be expected to contribute to overall arousal, while synaptic transmission acting via nAChRs could contribute to selective attention.

ACKNOWLEDGMENTS

This work was funded by the Swedish Research Council (project numbers 3050 and 2862) and Linköping University. The authors would like to thank Erik Johansson for assistance with FoxP2 immunohistochemical staining.

CONFLICT OF INTEREST

The authors declare no competing interests, financial or other.

AUTHOR CONTRIBUTIONS

All authors had full access to the data in the study and take responsibility for the integrity of the data and the accuracy of the data analysis. Study concept and design: S.C.S and B.G. Acquisition of data: S.C.S, S.H.L and G.M.S. Analysis and interpretation of data: S.C.S and B.G. Drafting of the manuscript: S.C.S, S.H.L and B.G. Statistical analysis: S.C.S and B.G. Obtained funding: B.G.

ORCID

Sofie Charlotte Sundberg http://orcid.org/0000-0002-5969-4313
Gonzalo Manuel Sanchez http://orcid.org/0000-0003-4415-1866
Sarah Helen Lindström http://orcid.org/0000-0001-7952-8120

REFERENCES

Ahlsén, G., Lindström, S., & Lo, F. S. (1985). Interaction between inhibitory pathways to principal cells in the lateral geniculate nucleus of the cat. *Experimental Brain Research*, *58*(1), 134–143.

Akk, G., & Steinbach, J. H. (2003). Activation and block of mouse muscle-type nicotinic receptors by tetraethylammonium. *Journal of Physiology*, *551*(Pt 1), 155–168. https://doi.org/10.1113/jphysiol.2003.043885

Bailey, C. D., Alves, N. C., Nashmi, R., De Biasi, M., & Lambe, E. K. (2012). Nicotinic α5 subunits drive developmental changes in the activation and morphology of prefrontal cortex layer VI neurons. *Biological Psychiatry*, *71*(2), 120–128. https://doi.org/10.1016/j.biopsych.2011.09.011

Bortone, D. S., Olsen, S. R., & Scanziani, M. (2014). Translaminar inhibitory cells recruited by layer 6 corticothalamic neurons suppress visual cortex. *Neuron*, *82*(2), 474–485. https://doi.org/10.1016/j.neuron.2014.02.021

Bowers, J. M., Perez-Pouchoulen, M., Roby, C. R., Ryan, T. E., & McCarthy, M. M. (2014). Androgen modulation of Foxp1 and Foxp2 in the developing rat brain: Impact on sex specific vocalization. *Endocrinology*, *155*(12), 4881–4894. https://doi.org/10.1210/en.2014-1486

Briggs, F. (2010). Organizing principles of cortical layer 6. *Frontiers in Neural Circuits*, *4*, 3. https://doi.org/10.3389/neuro.04.003.2010

Brumberg, J. C., Hamzei-Sichani, F., & Yuste, R. (2003). Morphological and physiological characterization of layer VI corticofugal neurons of mouse primary visual cortex. *Journal of Neurophysiology*, *89*(5), 2854–2867. https://doi.org/10.1152/jn.01051.2002

Case, L., Lyons, D. J., & Broberger, C. (2016). Desynchronization of the rat cortical network and excitation of white matter neurons by neurotensin. *Cerebral Cortex*, *27*, 2671–2685. https://doi.org/10.1093/cercor/bhw100

Chattopadhyaya, B., Di Cristo, G., Higashiyama, H., Knott, G. W., Kuhlman, S. J., Welker, E., & Huang, Z. J. (2004). Experience and activity-dependent maturation of perisomatic GABAergic innervation in primary visual cortex during a postnatal critical period. *Journal of Neuroscience*, *24*(43), 9598–9611. https://doi.org/10.1523/JNEUROSCI.1851-04.2004

Cotel, F., Apergis-Schoute, J., & Williams, R. (2014). Intra-cortical excitatory circuitry innervating layer 6 pyramidal neurons of the rat primary visual cortex. SFN abstract, 532.09.

Crandall, S. R., Cruikshank, S. J., & Connors, B. W. (2015). A corticothalamic switch: Controlling the thalamus with dynamic synapses. *Neuron*, *86*(3), 768–782. https://doi.org/10.1016/j.neuron.2015.03.040

Denman, D. J., & Contreras, D. (2015). Complex effects on in vivo visual responses by specific projections from mouse cortical layer 6 to dorsal lateral geniculate nucleus. *Journal of Neuroscience*, *35*(25), 9265–9280. https://doi.org/10.1523/JNEUROSCI.0027-15.2015

Descarries, L., Gisiger, V., & Steriade, M. (1997). Diffuse transmission by acetylcholine in the CNS. *Progress in Neurobiology*, *53*(5), 603–625.

Gong, S., Doughty, M., Harbaugh, C. R., Cummins, A., Hatten, M. E., Heintz, N., & Gerfen, C. R. (2007). Targeting Cre recombinase to specific neuron populations with bacterial artificial chromosome constructs. *Journal of Neuroscience*, *27*(37), 9817–9823. https://doi.org/10.1523/JNEUROSCI.2707-07.2007

Granseth, B. (2004). Dynamic properties of corticogeniculate excitatory transmission in the rat dorsal lateral geniculate nucleus in vitro. *Journal of Physiology*, *556*(Pt 1), 135–146. https://doi.org/10.1113/jphysiol.2003.052720

Guillem, K., Bloem, B., Poorthuis, R. B., Loos, M., Smit, A. B., Maskos, U., … Mansvelder, H. D. (2011). Nicotinic acetylcholine receptor β2 subunits in the medial prefrontal cortex control attention. *Science*, *333*(6044), 888–891. https://doi.org/10.1126/science.1207079

Gulledge, A. T., Park, S. B., Kawaguchi, Y., & Stuart, G. J. (2007). Heterogeneity of phasic cholinergic signaling in neocortical neurons. *Journal of Neurophysiology*, *97*(3), 2215–2229. https://doi.org/10.1152/jn.00493.2006

Hay, Y. A., Lambolez, B., & Tricoire, L. (2015). Nicotinic transmission onto layer 6 cortical neurons relies on synaptic activation of non-α7 receptors. *Cerebral Cortex*, *26*, 2549–2562. https://doi.org/10.1093/cercor/bhv085

Hedrick, T., & Waters, J. (2015). Acetylcholine excites neocortical pyramidal neurons via nicotinic receptors. *Journal of Neurophysiology*, *113*(7), 2195–2209. https://doi.org/10.1152/jn.00716.2014

Hisaoka, T., Nakamura, Y., Senba, E., & Morikawa, Y. (2010). The forkhead transcription factors, Foxp1 and Foxp2, identify different subpopulations of projection neurons in the mouse cerebral cortex. *Neuroscience*, *166*(2), 551–563. https://doi.org/10.1016/j.neuroscience.2009.12.055

Hu, J., Matsui, M., Gagnon, K. T., Schwartz, J. C., Gabillet, S., Arar, K., … Corey, D. R. (2009). Allele-specific silencing of mutant huntingtin and ataxin-3 genes by targeting expanded CAG repeats in mRNAs. *Nature Biotechnology*, *27*(5), 478–484. https://doi.org/10.1038/nbt.1539

Kim, J., Matney, C. J., Blankenship, A., Hestrin, S., & Brown, S. P. (2014). Layer 6 corticothalamic neurons activate a cortical output layer, layer 5a. *Journal of Neuroscience*, *34*(29), 9656–9664. https://doi.org/10.1523/JNEUROSCI.1325-14.2014

Krnjević, K., Pumain, R., & Renaud, L. (1971). The mechanism of excitation by acetylcholine in the cerebral cortex. *Journal of Physiology*, *215*(1), 247–268.

Lambe, E. K., Picciotto, M. R., & Aghajanian, G. K. (2003). Nicotine induces glutamate release from thalamocortical terminals in prefrontal cortex. *Neuropsychopharmacology*, *28*(2), 216–225. https://doi.org/10.1038/sj.npp.1300032

Meijering, E., Jacob, M., Sarria, J. C., Steiner, P., Hirling, H., & Unser, M. (2004). Design and validation of a tool for neurite tracing and analysis in fluorescence microscopy images. *Cytometry A*, *58*(2), 167–176. https://doi.org/10.1002/cyto.a.20022

Mercer, A., West, D. C., Morris, O. T., Kirchhecker, S., Kerkhoff, J. E., & Thomson, A. M. (2005). Excitatory connections made by presynaptic cortico-cortical pyramidal cells in layer 6 of the neocortex. *Cerebral Cortex*, *15*(10), 1485–1496. https://doi.org/10.1093/cercor/bhi027

Mrzljak, L., Pappy, M., Leranth, C., & Goldman-Rakic, P. S. (1995). Cholinergic synaptic circuitry in the macaque prefrontal cortex. *Journal of Comparative Neurology*, *357*(4), 603–617. https://doi.org/10.1002/cne.903570409

Olsen, S. R., Bortone, D. S., Adesnik, H., & Scanziani, M. (2012). Gain control by layer six in cortical circuits of vision. *Nature*, *483*(7387), 47–52. https://doi.org/10.1038/nature10835

Schneider, C. A., Rasband, W. S., & Eliceiri, K. W. (2012). NIH Image to ImageJ: 25 years of image analysis. *Nature Methods*, *9*(7), 671–675.

Steriade, M. (2004). Acetylcholine systems and rhythmic activities during the waking–sleep cycle. *Progress in Brain Research*, *145*, 179–196. https://doi.org/10.1016/S0079-6123(03)45013-9

Tasic, B., Menon, V., Nguyen, T. N., Kim, T. K., Jarsky, T., Yao, Z., … Zeng, H. (2016). Adult mouse cortical cell taxonomy revealed by single cell transcriptomics. *Nature Neurosciences*, *19*(2), 335–346. https://doi.org/10.1038/nn.4216

Thiele, A. (2013). Muscarinic signaling in the brain. *Annual Review of Neuroscience*, *36*, 271–294. https://doi.org/10.1146/annurev-neuro-062012-170433

Thomson, A. M. (2010). Neocortical layer 6, a review. *Frontiers in Neuroanatomy*, *4*, 13. https://doi.org/10.3389/fnana.2010.00013

Velez-Fort, M., Rousseau, C. V., Niedworok, C. J., Wickersham, I. R., Rancz, E. A., Brown, A. P., ... Margrie, T. W. (2014). The stimulus selectivity and connectivity of layer six principal cells reveals cortical microcircuits underlying visual processing. *Neuron*, *83*(6), 1431–1443. https://doi.org/10.1016/j.neuron.2014.08.001

Vinson, P. N., & Justice, J. B. (1997). Effect of neostigmine on concentration and extraction fraction of acetylcholine using quantitative microdialysis. *Journal of Neuroscience Methods*, *73*(1), 61–67.

Xiang, Z., Huguenard, J. R., & Prince, D. A. (1998). Cholinergic switching within neocortical inhibitory networks. *Science*, *281*(5379), 985–988.

How to cite this article: Sundberg SC, Lindström SH, Sanchez GM, Granseth B. Cre-expressing neurons in visual cortex of Ntsr1-Cre GN220 mice are corticothalamic and are depolarized by acetylcholine. *J Comp Neurol*. 2018;526:120–132. https://doi.org/10.1002/cne.24323